Nat Hazards (2014) 74:155–177
DOI 10.1007/s11069-014-1193-5

ORIGINAL PAPER

The Lake Michigan meteotsunamis of 1954 revisited

Adam J. Bechle · Chin H. Wu

Received: 21 August 2013 / Accepted: 14 April 2014 / Published online: 23 April 2014
© Springer Science+Business Media Dordrecht 2014

Abstract Two large meteotsunami wave events on Lake Michigan impacted the Chicago coastline within 10 days of each other in 1954. Initial data analysis suggested that the fatal first event (June 26) was caused by a Proudman resonant non-trapped wave, while the second event (July 6) was caused by Greenspan resonant trapped edge waves. In this study, a numerical hydrodynamic model was used to reveal the detailed behavior of these events. For both events, the atmospheric pressure and wind perturbations were found to be essential to explain the magnitude of the wave activity, in contrast to the initial conclusions that the waves were primarily pressure-driven. In the June 26 meteotsunami, Proudman resonance wave was the primary cause of the destructive wave, though the storm also generated edge waves which persisted for many hours, hindering rescue efforts. The maximum wave heights for the July 6 event were found to be the product of a superposition of edge waves and non-trapped waves rather than purely edge waves as originally thought. The results from these events demonstrate the enclosed Lake Michigan basin retained and focused wave energy, leading to their large magnitude, long duration, and destructive nature.

Keywords Meteotsunami · Proudman resonance · Greenspan resonance · Non-trapped wave · Edge wave · Lake Michigan · Hydrodynamic modeling

1 Introduction

In the summer of 1954, the Chicago coastline was impacted by two large tsunami-like wave incidents just 10 days apart. On June 26, 1954, a large wave occurred at the coast of Lake Michigan near Chicago, with heights of up to 3 m reported in some locations (Ewing et al. 1954). The wave initially struck the north shore of Chicago and swept many

A. J. Bechle · C. H. Wu (✉)
Department Civil and Environmental Engineering, University of Wisconsin, 1261B Engineering Hall, Madison, WI 53706, USA
e-mail: chinwu@engr.wisc.edu

fishermen off of piers at Montrose Harbor, with a total of seven people drowning. News of the wave spread quickly along the lakefront, and police and lifeguards cleared people from the waterfront, where many beaches were inundated up to 50 m inland. Strong oscillations persisted in the lake long after the disaster, with the Chicago Daily News reporting that rescue and recovery efforts were hindered by strong currents for up to 34 h after the initial wave arrival. Just 10 days later, on July 6, another series of large waves impacted the Chicago shoreline, with a maximum recorded wave height exceeding 1.25 m, followed by 0.3 m waves which persisted for over 24 h (Donn and Ewing 1956). In fact, the harbormaster at Belmont Harbor reported to the Chicago Tribune that lake conditions on July 6th meteotsunami were much more severe than on June 26th. Fortunately, owing to the heightened awareness from the fatal event 10 days prior, sufficient warnings were issued and no loss of life occurred (Hughes 1965). Both events exhibited tsunami-like behavior and were revealed to be meteorologically induced. For that reason, they are called meteorological tsunamis, or meteotsunamis (Monserrat et al. 2006). Nevertheless, major disparities in the metrological forcings of these two events caused the subsequent meteotsunami waves to have quite different behaviors.

The June 26, 1954 meteotsunami was associated with a squall line storm with wind of approximately 25 m/s and a rapid jump in atmospheric pressure of approximately 300 Pa over 4 min. From the arrival times of the pressure disturbance at meteorological stations around the lake, the squall line was determined to move across the lake at 29 m/s with a direction of 135° from north (Ewing et al. 1954). The propagation pathway coincided with a long stretch of water depths between 75 and 90 m (Fig. 1), corresponding to an estimated wave speed of 27–30 m/s. Ewing et al. (1954) deduced that the large wave event was caused by Proudman resonance (Proudman 1929), which occurs when the atmospheric disturbance speed matches that of the wave speed such that atmospheric energy is constantly fed into the water wave, growing amplitude by up to an order of magnitude. The amplified wave first impacted the southeast coast of the lake, where wave heights of 1.5–2 m were reported. The wave then reflected off of the coast, returned westward across the lake, and finally struck the Chicago lakefront with a destructive 3 m magnitude. The assertion of Proudman resonance by Ewing et al. (1954) was supported by numerical modeling of the event by Platzman (1958). Specifically, the moving speed of the squall line was perturbed in multiple simulations, with the maximum amount of energy transmitted to the lake by a squall line moving at 29 m/s, suggesting that the June 26, 1954 meteotsunami event may have been a worst-case scenario of Proudman resonance. Nevertheless, this early modeling study was limited in resolution, as the 4 km grid did not resolve significant higher-frequency wave content ($T \sim 10$ min) that appeared in the observations. In addition, the model atmospheric disturbance only considered atmospheric pressure fluctuations while excluding the wind forcing, yielding wave heights that underpredicted the observations by a factor of two. Platzman (1965) used this model to conduct a sensitivity study of the response of Lake Michigan to a generic pressure and wind forcing, producing nomograms of maximum wave height and wave arrival time with respect to various disturbance speeds and directions. These nomograms suggest that wind stress, which was neglected in the model of Platzman (1958), was responsible for over half of the wave energy of the destructive June 26 meteotsunami. While these results provide insight into the general behavior of meteotsunamis in Lake Michigan, Platzman (1965) recognized the limitations of the "rudimentary" representation of pressure and wind forcings. Furthermore, Platzman (1965) suggested constructing meteorological forcings from observations combined with a higher-resolution computational grid to reveal the true character of these waves. Overall, the findings in Ewing et al. (1954), Platzman (1958), and Platzman (1965)

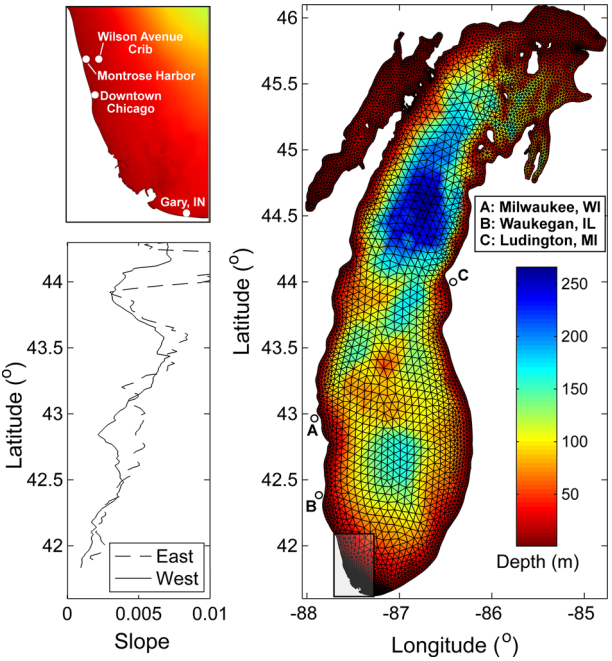

Fig. 1 Unstructured model grid mesh overlaid on Lake Michigan bathymetry. *Bottom* slopes along the west and east coasts are shown at the *bottom–left*; and at the *top–left* is a zoomed view of the coast near the Chicago lakeshore

laid out a basic understanding of the devastating June 26, 1954 Lake Michigan meteotsunami. Nevertheless, important aspects of the wave behavior have remained unresolved, including the final wave magnitude, observed high-frequency waves, and long-lasting oscillations.

The July 6, 1954 meteotsunami was associated with a large pressure jump propagating over the lake, though with a much different character than the squall line which occurred 10 days prior (Donn and Ewing 1956). The atmospheric pressure raised 350 Pa over a period of 30 min and then decreased by 500 Pa over the next 4 h. The pressure fluctuation was accompanied by strong northern winds of 30 m/s over a similar time scale. Isochrones for this event indicate that the pressure fluctuation propagated at 22 m/s in a direction of 155° from north. Compared to the June 26th event, this atmospheric disturbance propagated slower and in a more meridional direction with a much more gradual pressure fluctuation. The passage of the pressure fluctuations coincided with large waves along the west coast of the lake, with the wave height in excess of 1.25 m observed near Chicago. Donn and Ewing (1956) concluded that these oscillations were edge waves, which are waves trapped to the coast by topographic refraction. The speed of edge waves, c_{edge}, is governed by the dispersion relationship

$$c_{\text{edge}} = gT \tan[\beta(2n+1)]/2\pi \tag{1}$$

where β is the lake bottom slope, T is the edge wave period, and g is the acceleration due to gravity (Ursell 1952). Based on the average bottom slope of $\beta = 0.0022$ along the southwest coast of Lake Michigan calculated at the 50 m contour (Fig. 1) and an

observed wave period of 110 min, the estimated edge wave speed is 23 m/s, nearly identical to the atmospheric disturbance speed. Thus, the large magnitude of the waves was attributed to a match between the speed of the atmospheric disturbance and the edge waves; known as Greenspan resonance (Greenspan 1956). The modeling results of Platzman (1965) indicated that a storm of this speed and direction would generate edge waves of approximately 1 m in magnitude, with wind stress as the dominant forcing. Nevertheless, the arrival time of the waves after the passing of the storm predicted by Platzman (1965) (120 min) is much greater than was observed (34 min), likely owing to the generic pressure and wind forcings used to drive the model which deviate greatly from the recorded meteorology. In addition, maximum wave heights in the observations were not achieved in the first wave arrival, as would be expected from pure Greenspan edge wave resonance (Greenspan 1956). Instead, the maximum wave height occurred with the second wave, suggesting that interaction between multiple waves may have occurred in this event. Donn and Ewing (1956) also observed small shorter period waves ($H \sim 0.15$ m, $T \sim 20$ min) superposed on top of the larger edge waves, but no resolute explanation for these oscillations was made. Despite producing large waves, the July 6th wave did not garner much attention compared with the fatal June 26th meteotsunami. As a result, our understanding of this edge wave resonance has been limited to the data analysis of Donn and Ewing (1956) and generic modeling of Platzman (1965). Many features of the July 6 meteotsunami remain unknown, including the nature of the resonant wave growth, the occurrence of the maximum waves later in the wave train, and the source of the high-frequency waves.

The overall objective of this paper is to address the uncertainties regarding the atmospheric forcing, wave growth, high-frequency fluctuations, and the long duration of the oscillations of these two historic Lake Michigan meteotsunami events. First, we address the relative weighting between atmospheric pressure and wind stress on the meteotsunami generation. Whereas for most observed meteotsunamis, the wind speeds have not been great enough to dominate the wave behavior (Vilibić et al. 2005; Orlić et al. 2010; Renault et al. 2011), the modeling sensitivity study by Platzman (1965) in Lake Michigan suggested that the wind speeds in these events did contribute to a significant portion of the meteotsunami energy. Nevertheless, as the "rudimentary" implementations of pressure and wind speed recognized by Platzman (1965) do not faithfully represent the meteorology of these events, we examine the response of the lake to the observed meteorological forcings. Second, we aim to explain the character of the wave growth, specifically the largest wave in the July 6th event which occurred in the middle of the wave train. Furthermore, the sensitivity of the wave growth mechanisms to atmospheric disturbance orientation and speed is explored. Third, we investigate the significant higher-frequency content of these meteotsunami events ($T < 20$ min) that were not explained by the effects of Proudman and Greenspan resonances (Ewing et al. 1954; Donn and Ewing 1956). Finally, we aim to explain the long duration of the water level oscillations in these meteotsunamis, specifically the unexpectedly long-lasting waves present in the June 26th event.

The paper is structured as follows. Section 2 details the hydrodynamic modeling and atmospheric data. In Sect. 3, the results are presented for the two meteotsunami events, June 26 and July 6, 1954. In Sect. 4, salient features of these meteotsunamis are discussed to address the aforementioned uncertainties that remain for these events. Finally, conclusions are drawn in Sect. 5.

2 Hydrodynamic modeling and data

The hydrodynamic model semi-implicit Eulerian–Lagrangian finite element (SELFE) (Zhang and Baptista 2008a; Zhang et al. 2011) is employed in this paper. SELFE is a well-validated model and has been used to study hurricane response (Cho et al. 2012), tsunami propagation (Zhang and Baptista 2008b; Zhang et al. 2011), and inundation (Witter et al. 2011; Fortunato et al. 2013). SELFE solves the three-dimensional Reynolds-averaged Navier–Stokes equations

$$\frac{\partial u}{\partial x}+\frac{\partial v}{\partial y}+\frac{\partial w}{\partial z}=0 \tag{2}$$

$$\frac{\mathrm{d}u}{\mathrm{d}t}=fv+\frac{\partial}{\partial x}(g\eta)+\frac{\partial}{\partial x}\left(\frac{P_{\mathrm{a}}}{\rho_o}\right)+\frac{\partial}{\partial z}\left(K_m\frac{\partial u}{\partial z}\right)+\frac{\partial}{\partial x}\left(F_x\frac{\partial u}{\partial x}\right)+\frac{\partial}{\partial y}\left(F_y\frac{\partial v}{\partial y}\right) \tag{3}$$

$$\frac{\mathrm{d}v}{\mathrm{d}t}=-fu+\frac{\partial}{\partial y}(g\eta)+\frac{\partial}{\partial y}\left(\frac{P_{\mathrm{a}}}{\rho_o}\right)+\frac{\partial}{\partial z}\left(K_m\frac{\partial v}{\partial z}\right)+\frac{\partial}{\partial x}\left(F_x\frac{\partial u}{\partial x}\right)+\frac{\partial}{\partial y}\left(F_y\frac{\partial v}{\partial y}\right) \tag{4}$$

$$\frac{\partial \eta}{\partial t}+\frac{\partial}{\partial x}\int_{-h}^{\eta}u\,\mathrm{d}z+\frac{\partial}{\partial y}\int_{-h}^{\eta}v\,\mathrm{d}z=0 \tag{5}$$

where x, y, and z are Cartesian coordinates; u, v, and w are velocity components; ρ_o is density; η is free-surface elevation; h is the bathymetric depth; P_{a} is surface atmospheric pressure; g is gravitational acceleration; f is Coriolis factor; K_m is vertical eddy viscosity; and F_x and F_y are horizontal eddy viscosity. Wind stress is applied at the surface boundary and is calculated from a quadratic drag formulation:

$$K_m\left(\frac{\partial u}{\partial z},\frac{\partial v}{\partial z}\right)=\frac{\rho_{\mathrm{a}}}{\rho_o}C_{\mathrm{D}}|W|\left(W_x,W_y\right)\ \ \text{at}\ z=\eta \tag{6}$$

where $|W|$ is the magnitude of the wind speed, (W_x, W_y) are the wind speed components, ρ_a is the density of air, ρ_o is the density of water at the surface, and C_{D} is the drag coefficient. A linear relationship between drag coefficient and wind speed is assumed (Sheppard 1958), as the winds used in this study approach but do not exceed observed drag coefficient saturation thresholds, above which linearity breaks down (Powell et al. 2003; Donelan et al. 2004); specifically, the empirical linear relationship used is that of Smith (1980). Bottom friction is applied at the bottom boundary and is calculated from the quadratic drag law:

$$K_m\left(\frac{\partial u}{\partial z},\frac{\partial v}{\partial z}\right)=C_f\sqrt{u^2+v^2}(u,v)\ \text{at z}\ =-h \tag{7}$$

where C_f is the bottom drag coefficient. The governing equations are solved on an unstructured horizontal grid with a hybrid S–Z vertical coordinate system. A Galerkin finite element scheme is used to solve the pressure gradient, while advection terms are treated with a higher-order Eulerian–Lagrangian scheme. Semi-implicit time-stepping is used to avoid mode splitting and allow for large time steps.

The model domain encompasses the entire Lake Michigan basin. The horizontal grid is a triangular unstructured mesh with a resolution ranging from 1,000 m in the open water down to 30 m along some sections of the coast, yielding 109,892 computational elements. The vertical grid is composed of 10 layers (Song and Haidvogel 1994). A time step of $\Delta t = 25$ s is chosen based on the semi-implicit scheme. A bottom drag coefficient of

$C_f = 0.0025$ is used based on calibration against water level results from the Great Lake Coastal Forecasting Model (Kelley et al. 1998; O'Connor et al. 1999) (not be shown here for brevity). The model is forced with moving disturbances of atmospheric pressure and wind stress constructed to emulate historical observations of the two meteotsunami events. The atmospheric pressure gradients characteristic of meteotsunami-causing disturbances is calculated based upon an integral approach in which the line integral of pressure around the perimeter of each computational element is used to calculate the pressure gradient of the element. As the atmospheric disturbances in this study are approximated by analytical definitions, these line integrals can be calculated numerically with high precision to give a better representation of the rapidly varying pressure disturbance than the original vertex-based gradient calculation in SELFE.

The first event is the June 26, 1954 meteotsunami, caused by a squall line thunderstorm propagating across the lake. Atmospheric pressure and wind speed observations of this event from the Wilson Avenue Crib meteorological station (see Fig. 1 for location) were originally published by Platzman (1958), shown as black lines in Fig. 2. Atmospheric pressure experienced a rapid increase of 300 Pa over a period of 4 min starting at 6:25 Central Standard Time (all subsequent times are in CST), maintained a constant pressure over 90 min, and ended with a slow 200 Pa decrease over an additional 90 min. Wind speed sharply increased to 25 m/s over the course of a minute with the arrival of the squall line at 6:21 and subsequently decreased to zero over a period of 30 min. In the model, we approximated the atmospheric pressure disturbance spatially as a trapezoidal pressure perturbation (blue lines in Fig. 2), with an initial 300 Pa increase over 7 km, 160 km of constant pressure, and a 200 Pa decline over a subsequent 160 km. Similarly, the wind stress of the squall line was represented using a triangular wind speed perturbation, with an initial 25 m/s increase over 2 km and a 25 m/s decline over a subsequent 54 km. Due to limited available spatial information, both the atmospheric pressure and wind speed perturbations were assumed to be a straight linear front constant over the lake and propagated at 29 m/s at a direction 135° from north (Ewing et al. 1954).

The second meteotsunami occurred on July 6, 1954, and was associated with a pressure disturbance, though strong winds were also noted. Pressure observations of this event from the Wilson Avenue Crib meteorological station were originally published by Donn and Ewing (1956), shown as a black line in Fig. 3. An increase in atmospheric pressure of 350 Pa occurred over a period of 30 min starting at 15:02, followed by a much slower 500 Pa decrease in pressure over an additional 4 h. The atmospheric pressure disturbance was spatially approximated as a triangular pressure perturbation (blue line in Fig. 3), with an initial 350 Pa pressure increase over 40 km and a 500 Pa decline in pressure over a subsequent 315 km. Donn and Ewing (1956) did not report wind anemometer data though wind speed was noted to have sharply increased from 10 to 32 m/s over the 30-min period of pressure rise. The best available data for this event are from the hourly wind record at the Glenview Naval Air Station (shown as dots in Fig. 3), which confirm this wind speed but are temporally too coarse to infer more detail about the wind field. Based on the descriptions of the wind behavior by Donn and Ewing (1956), a triangular wind speed perturbation is assumed here with an increase in wind to 32 m/s over 40 km and a subsequent decrease back to 10 m/s over an additional 80 km, shown as a blue line in Fig. 3. Both the atmospheric pressure and wind speed perturbations are assumed to be a straight linear front constant over the lake and are propagated across the model domain at 22 m/s at a direction 155° from north, in accordance with the observations by Donn and Ewing (1956).

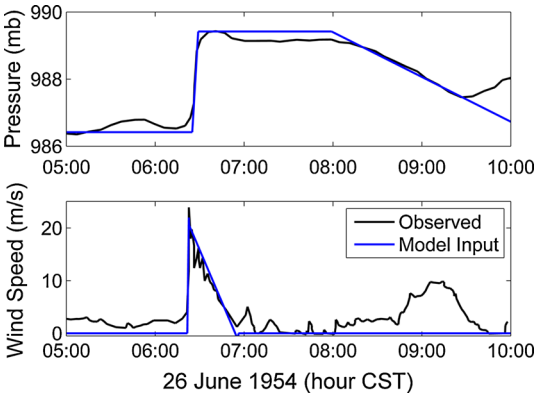

Fig. 2 Observed June 26, 1954 atmospheric pressure and wind records (*black lines*) at Wilson Avenue Crib station (taken from (Platzman 1958)) and corresponding input meteorological forcing functions (*blue lines*) used for the hydrodynamic model

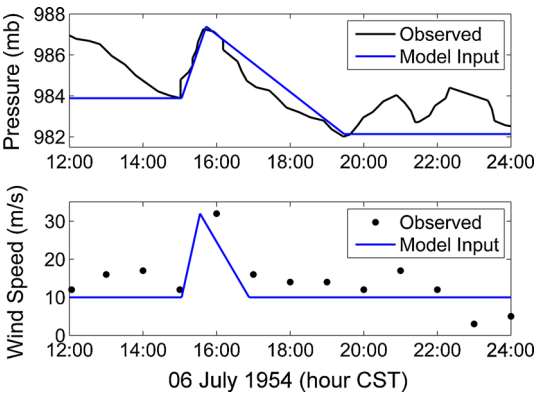

Fig. 3 Observed July 6, 1954 atmospheric pressure records at Wilson Avenue Crib station (taken from Donn and Ewing 1956) and hourly wind records available at the Glenview Naval Air Station, IL. The blue lines are the input meteorological forcing functions for hydrodynamic model

3 Results

3.1 June 26, 1954 Meteotsunami

Model results are first compared with the water level observations at Wilson Avenue Crib (Fig. 4), located at (41.97°N, 87.59°W), 4 km east of Montrose Harbor where the main disaster occurred (Platzman 1958). Since Wilson Avenue Crib was the only open-water water level station to record the June 26, 1954 meteotsunami, these observations provide insight into the nature of the propagating meteotsunami wave, unlike shore-based gauges which can be adulterated by local mechanisms such as harbor oscillations (Rabinovich 2009). To elucidate the importance of pressure and wind on the meteotsunami formation, we run the model for three separate forcing scenarios: (1) pressure only, (2) wind only, and (3) pressure and wind. Figure 4 shows that neither the pressure nor wind forcing alone is sufficient to reach the magnitude of the water level oscillations, but the wave height resulting from the combination of both pressure and wind forcing closely matches the observed wave time series. Interestingly, the time series resulting from a superposition of the "pressure only" and "wind only" records is nearly identical to the time series of the simultaneous pressure and wind forcing scenario, suggesting that the wave behaves in a linear manner. Pressure accounted for approximately 60 % of the wave height, and wind

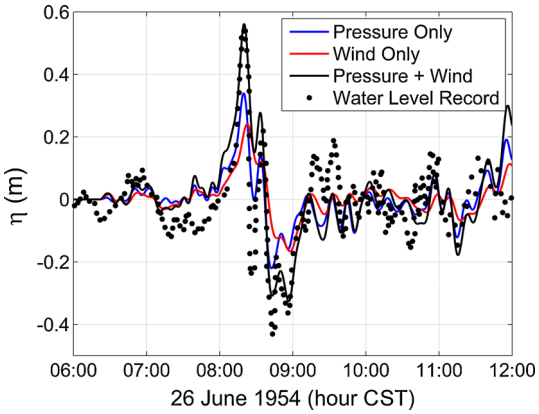

Fig. 4 Time series of modeled water levels (*line*) and observations (*dot*) at Wilson Avenue Crib in response to the meteorological forcings on June 26, 1954, from Fig. 2

stress contributed the remaining 40 % of the event. This finding agrees with an analytical comparison of the pressure and wind terms of Eqs. 2 and 3; the atmospheric pressure term is calculated as $\partial(P_a/\rho)/\partial x$, the fourth term of Eq. 2, whereas the wind term is $\tau/\rho H$, derived from fifth term of Eq. 2 where wind stress, τ, is calculated from the formulation of Eq. 6, and the vertical derivative is taken as a linear gradient over depth, H (Orlić et al. 2010). From the pressure rise of 300 Pa over 7 km, the pressure term is 4.3×10^{-5} m/s^2, and from a maximum wind speed of 25 m/s over a resonant depth of 80 m, the wind term is 2.1×10^{-5} m/s^2. This analytical analysis attributes 67 % of the wave height to pressure and 32 % to wind, which is a greater imbalance than depicted in the model. Nevertheless, as shown in Fig. 2, the pressure gradient rise acted over 4 min, while the wind speed varied linearly over 30 min. To account for the effects of the different pressure and wind disturbance forms, these two terms are integrated over the pressure and wind perturbations of Fig. 2. When averaged over the duration of the perturbations, the pressure term is 7.2×10^{-6} m/s^2 and wind is 5.7×10^{-6} m/s^2. This yields a pressure and wind partitioning of 56 and 44 %, respectively, closer to the model result of 60 %/40 % split between pressure and wind. As the wind term is dependent upon depth, wind is expected to have a greater influence than pressure over depths shallower than 60 m (see Fig. 1) (Orlić et al. 2010), though subsequently slower shallow water speeds ($c < 24$ m/s) would not promote significant Proudman resonance (Platzman 1958). The model of Platzman (1965), which forced the lake with generic pressure and wind disturbances, suggested that pressure accounted for 43 % of the wave height and wind for 57 %; the majority of the wave height is incorrectly attributed to wind stress because the Platzman (1965) model was forced with a both lower pressure gradient and a longer-duration wind stress field than was observed in the actual disturbance. Thus, while generic atmospheric disturbances provide an approximate indication of meteotsunami behavior, properly represented meteorological conditions are crucial to capture detailed meteotsunami wave formation.

With both pressure and wind forcing included, the model represents the magnitude and arrival time (8:20) of the devastating initial wave and the subsequent oscillations ($t >$ 8:25) which the simulations of Platzman (1958) could not replicate. This result illustrates the importance of the higher-resolution grid used in this study ($\sim$1 km) compared to the coarse-resolution grid employed in Platzman (1958) ($\sim$4 km). The source of the first of these subsequent oscillations ($T = 15$ min) was initially thought to be a "second surge" indicative of a high-frequency wave front with the remaining oscillations ($T = 9$ min)

attributed to background lake-level fluctuations (Platzman 1958). The simulations in this study reveal the first subsequent oscillation (8:33) to be the non-trapped wave reflected off of the west coast of Lake Michigan and propagating eastward toward open water, while the successive oscillations that persisted for the duration of the reported water level record ($t > 9{:}15$) were a train of anticyclonic propagating edge waves. Details of these oscillations will be analyzed through the spatial wave propagation through the entire lake.

The spatial propagation of the meteotsunami wave in response to the combined pressure and wind forcing is given in series of snapshots in Fig. 5. The first snapshot at 6:30 depicts the non-trapped wave that has propagated with the squall line for nearly 100 min, resulting in a resonant growth in the open water to a 0.2 m crest height. The location of the largest crest height corresponds to the Proudman resonance depths of 75–90 m, where the shallow water wave speed closely matched the squall line speed. The lowest heights of this wave front occurred in the middle of the lake, i.e., between longitudes of 87.0°W and 86.5°W, corresponding to the deepest point in southern Lake Michigan with the water depth of 160 m (see Fig. 1). As a result, the disturbance did not meet the Proudman resonance condition at this location, and wave growth was limited. Fifteen minutes later at 6:45, two distinct waves existed between longitudes of 87.0°W and 86.5°W, where the leading wave travelled at the faster free wave speed of the 150 m deep water, and the trailing wave was the forced wave aligned with the squall line. Meanwhile, the northern edge of the wave front first impacted the east coast of the lake at (42.6°N, 86.4°W). By 7:00, much of the non-trapped wave impacted the east coast of the lake, while the northern extent of the wave (42.7°N, 86.4°W) already began to reflect back westward. At 7:15, the non-trapped wave hit the southeast shore of the lake, reaching crest heights of 0.65 m, while north of 42.2°N, the wave reflected off the coast and travelled westward. By 7:30, the incident non-trapped wave fully reflected off the east coast. As the reflected wave approached the Chicago lakeshore at 7:45, the large horizontal extent of the original non-trapped wave ($\sim$150 km) that spanned diagonally across the lake converged to approximately 50 km. This was caused by the concave shape of the east coast of Lake Michigan, which acted to focus on the reflected wave and direct the propagation toward Chicago. Between 8:00 and 8:15, the reflected wave crest was refracted by the bathymetry to align with the coastline (Hibiya and Kajiura 1982), reaching a maximum offshore wave crest height of 0.43 m. Finally, the reflected wave struck the Chicago lakefront at 8:30, with maximum wave heights in the model occurring less than 2 km south of Montrose Harbor where the seven fatalities occurred. As seen at 8:45, the non-trapped wave reflected off of the Chicago lakeshore and propagated back eastward. This phenomenon explains the high-frequency "second surge" observed by Platzman (1958) at 8:35 in the Wilson Avenue Crib water level record (Fig. 4). Indeed, this wave should be considered neither a second surge nor a high-frequency component of the meteotsunami but instead a reflected wave propagating in the offshore direction. The reflected wave gave the appearance of a high-frequency wave when described by Platzman (1958) because the water level record was taken from Wilson Avenue Crib, located 4 km offshore such that a reflected wave would appear rather quickly after the incident wave in the water level measurements. The 4 km grid of the model by Platzman (1958) was too coarse to resolve a reflected wave at this location, as the simulated Wilson Avenue Crib record was derived from a node adjacent to the model boundary. Thus, the cause of this apparent high-frequency fluctuation was mistaken as a "second surge" when in reality, the source of this oscillation was a reflected wave which was propagating offshore and did not contribute to the disaster at the coast.

A series of 0.5 m high waves occurred along the coast for many hours after the initial meteotsunami wave struck Chicago, starting at approximately 9:15 (Harris 1957). While

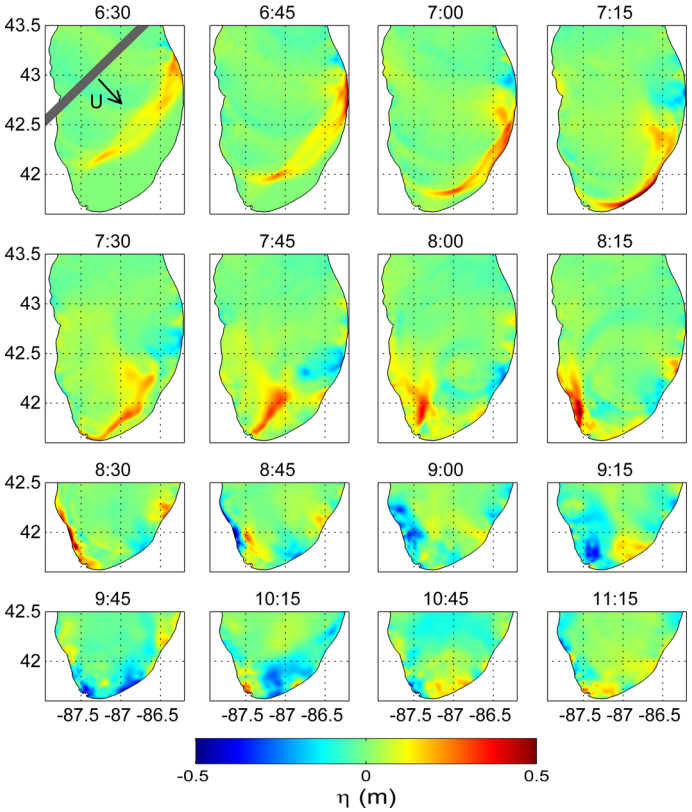

Fig. 5 Lake Michigan water level in response to meteorological forcings on June 26, 1954, from Fig. 2 (times are in CST)

these waves were not responsible for the drownings that occurred, the waves were still troublesome, as the Chicago Daily News reported that rescue and recovery efforts were hindered by strong currents and turbid waters that persisted for over a day. As seen in Fig. 5 between 8:45 and 9:15, a large portion of the wave energy caused by the Proudman resonance dissipated as the reflected non-trapped wave propagated back toward the eastern shore of Lake Michigan, likely owing to the convex shape of western coastline near Chicago where the wave reflected. Thus, the persistent oscillations were likely not due to a continual reflection of the destructive wave. The results of this simulation reveal that the long-lasting oscillations were instead an edge wave train generated by the squall line. Figure 5 at 6:30 shows that edge waves were generated by the squall line along the east coast at (43.1°N, 86.4°W). This edge wave structure has two alongshore antinodes, characteristic of the first harmonic edge wave mode (Ursell 1952). The existence of first harmonic edge waves is verified by calculating the expected wave speed based upon the edge wave dispersion relation given by Eq. 1, with the wave period of 12 min observed in the model, the bottom slope $\beta = 0.008$ from Fig. 1, and a mode number $n = 1$. The calculated speed of 29 m/s matches the disturbance propagation speed of 29 m/s, confirming the existence of first harmonic mode edge waves. As these harmonic edge waves travelled with the squall line, Greenspan resonance grew the waves to a relatively large

0.2 m crest height. A train of edge waves developed by 6:45, evident by the trough following the forced edge wave at (43.2°N, 86.6°W). By 7:00, the squall line crossed the shoreline and no longer travelled in resonance with the edge waves, resulting in a freely propagating edge wave train led by the 0.2 m trough at (43.1°N, 86.3°W). Between 7:00 and 7:45, the edge wave train encountered a slope change from $\beta = 0.006$ to $\beta = 0.002$. Free edge waves propagating over gradually shallowing slopes slow in celerity and increase height in an effect similar to shoaling (Kurkin and Pelinovsky 2003). Indeed, at 7:45, the edge wave velocity slowed to 15 m/s, and the trough reached a height of 0.38 m at (42.3°N, 86.3°W), exceeding the maximum height of the Proudman resonant wave which struck this location at 7:08. This evidence indicates the importance of the harmonic edge wave in this event, which was never reported before. As seen at 8:15, the edge wave reduced to a trough height of 0.25 m as the waves propagated around the convex shoreline near (42.1°N, 86.5°W). As the non-trapped wave meteotsunami wave struck the Chicago lakefront and reflected back into the open water, the edge wave train continued to propagate anticylonically around the lakeshore, eventually impacting the Chicago lakefront from 9:15 onward. This can also be seen in the Wilson Avenue Crib water level record (Fig. 4), in which oscillations persisted at this station for the extent of the record. The edge wave train revealed here likely explains the strong currents and turbid waters reported by the Chicago Daily News which impeded rescue and recovery efforts for over a day after the initial wave struck.

To verify the spatial patterns observed in the model snapshots, in Fig. 6, model results are compared with water level observations reported by Harris (1957) at shore-based gauges located at Milwaukee, WI; Waukegan, IL; Gary, IN; and Ludington, MI (see Fig. 1 for map of locations). Note that as the shore-based gauges are within harbors, the observed wave signal is likely masked by harbor oscillation modes (Rabinovich 2009). In this paper, the model grid does not resolve the scale of harbors at these locations, as simulating the interactions was not the intent. Nevertheless, a comparison of the observations with nearby model results provides an indication of wave magnitude and arrival time at the harbor. At Milwaukee (43.0°N, 87.9°W), which is 140 km north of Chicago, the model predicts an initial 0.25 m high wave arrival at 7:08, 15 min after the observed wave actually arrived with the similar magnitude. This oscillation is associated with a small edge wave train propagating along the west coast of the lake, visible in Fig. 6 at 7:15. While the main destructive wave did not extend north to Milwaukee, a 0.3 m wave appears in both the observation and model time series at approximately 9:00; this wave was a weak non-trapped wave reflection off the east coast of the lake and can be seen in Fig. 6 at 8:15 propagating to the northwest at (42.7°N, 87.8°W). Subsequent oscillations occurred at Milwaukee from 11:00 onward in both the observations and model results, attributed to the anticyclonic edge waves that were generated on the east coast of the lake. At Waukegan (42.4°N, 87.8°W), which is 70 km north of Chicago, the model predicts an initial wave arrival at 8:09 with crest height of 0.18 m followed by a second wave at 8:31 of 0.5 m height. Both waves can be seen in Fig. 6 at 8:15, with the first wave already at Waukegan and the second wave approaching the coast. The modeled waves arrived at Waukegan slightly ahead of the observed waves, which appeared in the record at 8:12 and 8:41 with similar magnitude. Subsequently, both the model and observations depict reasonably large ($H \sim 0.5$ m) oscillations for the remainder of the wave record ($t > 9{:}30$) at Waukegan which are the anticyclonic edge waves. At Gary (41.6°N, 87.3°W) near the southern extent of the lake, the model predicts a wave arrival at 8:38, which is well after the observed arrival at 8:12. Overall, the character of the observed water level time series is replicated by the model, specifically between 8:00 and 10:00 (corresponding to ~8:30 to 10:30 in

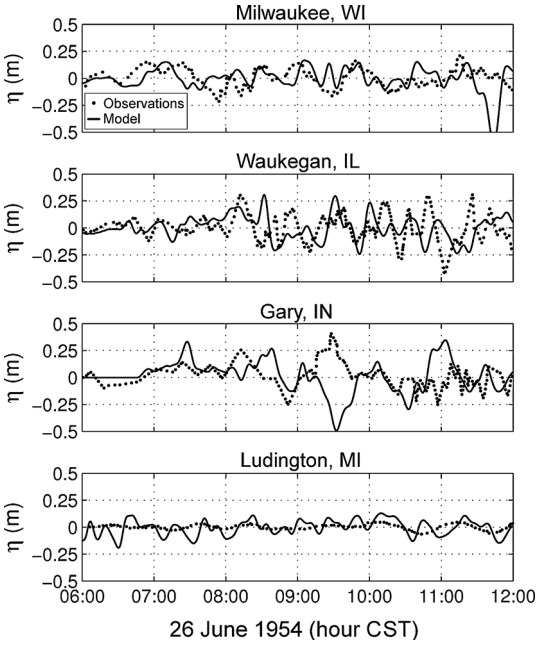

Fig. 6 Time series of modeled water levels (*line*) and observations (*dot*) at shore-based locations throughout Lake Michigan in response to the meteorological forcings on June 26, 1954. For gauge locations, see Fig. 1

model results), and this temporal discrepancy exists throughout the record. At Ludington (43.9°N, 86.5°W), which is located on the east side of the lake, waves of moderate height ($H \sim 0.2$ m) appear early in the model time series, associated with the passing of the simulated disturbance over Ludington at 5:40. Water level oscillations were not noticeable in the observations until 10:00. This discrepancy may be explained by the location of the water level gauge, which is separated from Lake Michigan by a harbor and a narrow channel, an arrangement which likely damped the small open lake oscillations. The oscillations that appear in the water level observations after 10:00 are revealed by the model to be a train of cyclonic edge waves. Overall, the model time series capture the nature of the water level observations well. The slight deviations in wave arrival times between the model and observations are likely due to the assumption of a straight linear disturbance front used in the model, whereas isochronal analysis of the event indicate that the front may have been slightly curved (Harris 1957). Nevertheless, over-lake surface meteorology observations are not available to accurately depict the actual shape of the disturbance. Discrepancies in oscillation frequency and magnitude are likely due to the harbors within which the observations were made, which were not resolved in the computational grid but modify the open water wave signal with local oscillation periods.

Finally, the sensitivity of the June 26th meteotsunami event to atmospheric disturbance velocity is examined by perturbing the simulated disturbance propagation direction. Platzman (1958) determined that meteotsunami wave energy wave for this event is maximized for a squall line moving at 29 m/s, concluding that this speed most effectively matches the non-trapped wave speed for Proudman resonance. The nomograms of Platzman (1965) provided further insight into the response of Lake Michigan to a combination of disturbance speeds and directions. In this paper, we aim to examine the detailed behavior of the June 26th event. Thus, the focus of this sensitivity is on the time series at Wilson Avenue Crib; for more general discussion of lake-wide response, readers are

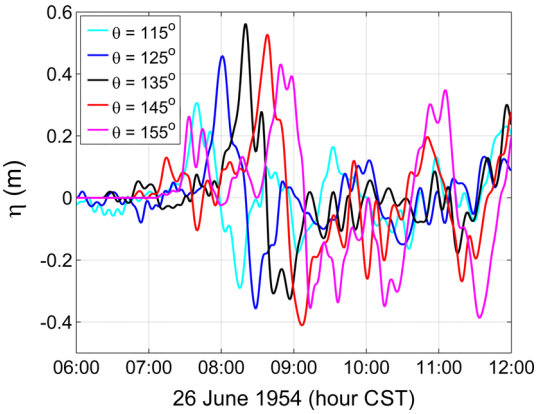

Fig. 7 Time series of water levels at Wilson Avenue Crib in response to perturbation of meteorological disturbance direction for the June 26, 1954 meteotsunami

referred to Platzman (1965). The propagation direction of the disturbance is perturbed in 10° increments, with the resulting water level time series at Wilson Avenue Crib plotted in Fig. 7. Compared with the actual event ($\theta = 135°$), a more zonal propagation pathway ($\theta = 125°$) results in an 8 % reduction in maximum wave height and an earlier wave arrival by 19 min. Subsequent oscillations are on the same order of magnitude as the original event. An even more zonal propagation ($\theta = 115°$) results in a 33 % reduction in the maximum wave height with a 40 min earlier arrival. A more meridional propagating storm ($\theta = 145°$) results in a 6 % increase in maximum wave height and an 18 min later arrival; this is consistent with the nomograms of Platzman (1965) which indicated the largest possible wave height would occur at this orientation. Spatial snapshots similar to Fig. 5 at 8:30 (not shown for brevity) reveal the extent of the Chicago coastline impacted by the destructive wave is minimized for $\theta = 145°$, suggesting that this disturbance orientation leads to the most optimal reflected wave focusing off of the concave east coast. This may explain why the 145° orientation of the event results in the largest wave magnitude. In addition, a pronounced 0.1 m wave crest appeared ahead of the destructive wave at 7:15, which is attributed to a forced edge wave caused by a disturbance orientation that is more perpendicular to the coast than the actual event. Large oscillations ($H \sim 0.4$ m) occurred after the destructive wave (10:00 and 11:00), which are anticyclonic edge waves generated on the east coast. An even more meridional propagation ($\theta = 155°$) yields a 12 % reduction in wave height and a later arrival time (8:50), but larger edge waves before (7:40, $H \sim 0.3$ m) and after (11:00, $H \sim 0.7$ m) the destructive non-trapped wave. Overall, the perturbations reveal that a slightly more meridional propagating storm (i.e., $\theta = 145$) on June 26th may have resulted in not only a larger non-trapped wave, but also much larger edge waves preceding and proceeding the disastrous event.

3.2 July 6, 1954 Meteotsunami

Model results for the July 6, 1954 meteotsunami are compared with the water level observations at Wilson Avenue Crib (see Fig. 8), originally reported by Donn and Ewing (1956). The relative role of pressure and wind in this event is assessed by forcing the model with pressure only, wind only, and combined pressure and wind scenarios. Figure 8 illustrates that the model with combined pressure and wind forcings matches the overall magnitude and phase of the water level fluctuations but underpredicts the maximum water

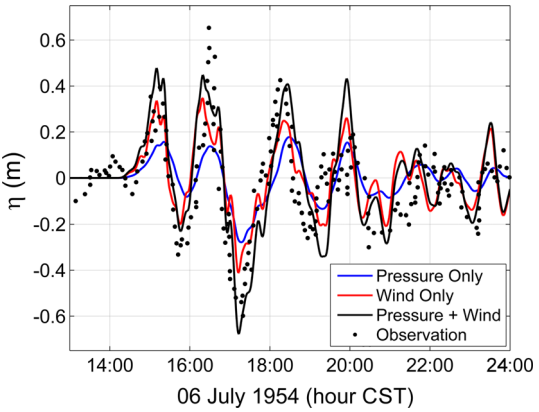

Fig. 8 Time series of modeled water levels (*line*) and observations (*dot*) at Wilson Avenue Crib in response to the meteorological forcings on July 6, 1954, from Fig. 3

level rise at 16:30. In addition, the model exhibits the high-frequency oscillations ($T \sim 20$ min) observed by Donn and Ewing (1956); these oscillations are due to a first harmonic edge wave mode, with more details provided later. In comparison with "pressure only" and "wind only" scenarios, the model with the combined forcings yields the better agreement with observations, in particular for the time between 15:30 and 19:00. Much like the June 26th event, the sum of the "pressure only" and "wind only" time series is almost equal to that of the simultaneously forced case, suggesting that nonlinear effects are negligible to the open water meteotsunami waves considered in this study. Nonlinear effects are expected to be more important in nearshore harbors where the waves would become steeper and more asymmetric (Vilibić et al. 2008), though these features were not resolved by the computational grid in this study. The result suggests that both pressure and wind forcings were essential to cause the water level oscillations, with wind stress as the dominant source of wave energy, accounting for 68 % of the wave height and pressure responsible for approximately 32 % of the wave height. The dominance of wind in this event is to be expected based on an analytical comparison of pressure and wind terms, owing to the shallower depths over which the edge waves propagate. From the pressure rise of 350 mb over 40 km, the pressure term of Eq. 2 is 8.8×10^{-6} m/s^2. As the main waves in this case were edge waves generated over coastal slopes, a maximum wind speed of 32 m/s is applied over the mean shelf depth of 25 m to give a wind term from Eq. 2 of 1.1×10^{-4} m/s^2. This partitioning would attribute only 7 % of the wave height to pressure and 93 % to wind, which is a greater imbalance than depicted in the model. As in Sect. 3.1, this estimate is revised by integrating and averaging the pressure and wind terms over the temporal perturbation forms in Fig. 3. This procedure yields a pressure term of 8.9×10^{-6} m/s^2 and wind term of $3.2 \times 10^{-5} \times$ m/s^2, and a pressure and wind partitioning of 22 and 78 %, respectively. This partitioning of wave energy source is similar to that found by Platzman (1965) for a disturbance of the same propagation speed and direction but narrower, generic pressure and wind forms, with 76 % of the wave height attributed to wind stress and 24 % to pressure. The major difference with the Platzman (1965) results, however, is the wave arrival times; whereas the nomogram of Platzman (1965) indicated that the wave train would arrive at Wilson Avenue Crib approximately 120 min after the disturbance passes, the model in this study simulates a 37-min lag in wave arrival, much closer to the observed 34 min and a critical improvement if such model results were to be used in a predictive capacity.

The spatial propagation of the July 6th meteotsunami is examined in detail in a series of snapshots in Fig. 9. By 13:45, the atmospheric disturbance generated edge waves on both the west and east coasts of the lake. At 43°N on the west coast, the slope is $\beta = 0.004$ (see Fig. 1), and the edge waves had a period of $T = 60$ min, yielding an edge wave speed of 23 m/s from Eq. 1, which is a near Greenspan resonant match with the atmospheric disturbance speed of 22 m/s. Along the east coast, slopes are too steep, i.e., $\beta = 0.007$ at 43.5°N, to experience Greenspan resonance, yielding a much small edge wave compared with the west coast. At 14:15, the leading edge wave along the west coast grew to a crest height of 0.34 m over constant slopes, and the edge wave train increased in duration. The length of an edge wave train continuously increases because edge wave group velocity is half the phase velocity, giving an edge wave train a duration that is equal to the length of time the edge waves have been propagating (Munk et al. 1956). Along the east coast, the edge waves grow over the shallower slope of $\beta = 0.005$ at 43.1°N, a more optimal condition for Greenspan resonance than to the north. At 14:45, the edge waves on the west coast grew to 0.6 m and a significant first harmonic component developed, evident by the offshore antinode. At this location along the west coast (42.1°N), the slope decreases to $\beta = 0.0035$ and the oscillations had a period of 20 min. These properties yield a first harmonic edge wave speed of 20 m/s from Eq. 1, a near Greenspan resonant match with the 22 m/s disturbance speed. Edge wave growth along the east coast became steady at this time with a 0.25 m crest height. In addition, non-trapped wave with a 0.2 m crest height formed across the lake, moving with the atmospheric disturbance. The lake depth in this area is 50–60 m, corresponding to a wave speed of 22–24 m/s which matched the disturbance speed to induce Proudman resonant wave growth. By 15:15, the west coast edge wave propagated to the Chicago lakefront with a crest height of 0.4 m, corresponding to the first wave arrival at the Wilson Avenue Crib gauge (see Fig. 8). The first harmonic edge wave mode was responsible for the high-frequency component ($T \sim 20$ min) of this first arrival wave in Fig. 8. Meanwhile, at the offshore, the wave grew to a crest height of 0.4 m as it propagated into shallower ($\sim$40 m) water depths. This wave growth is in agreement with the findings of Vilibić (2008) for a Proudman resonant wave which propagates over upward sloping bathymetry. Specifically, wave heights increase owing to shoaling, as well as the superposition of the forced wave, which maintains the disturbance speed, and a free wave which now travels slower over the shallower bathymetry. At 15:45, the leading west coast edge wave propagated south of Chicago with the trough of the edge wave train corresponding to the Wilson Avenue Crib low water level at 15:40 (Fig. 8). The non-trapped wave also impacted the southern coast of the lake, yielding water level fluctuations in which the non-trapped wave was indistinguishable from the cyclonic west coast edge waves. At 16:00, the non-trapped wave reflected off the southern coast of the lake and, as seen at 16:15, propagated northwest toward Chicago. Coincidently, an edge wave crest (42°N, 87.6°W) from the west coast edge wave train was also propagating toward Chicago at this time. This edge wave and the reflected non-trapped wave met at 16:30, leading to a superposed wave that was responsible for the largest peak (0.65 m) recorded at the Wilson Avenue Crib gauge, though the model results do not fully resolve this peak wave at Wilson Avenue Crib (see Fig. 8). This may be attributed to the use of a spatially homogenous atmospheric disturbance to force the model; in reality, the actual disturbance was undoubtedly spatially heterogeneous, though could not be characterized due to the limited available atmospheric data. Nevertheless, the model faithfully depicts the interactions of edge and non-trapped waves just 5 km south of the Wilson Avenue Crib gauge location with a resulting wave crest height of 0.7 m. Also at 16:30, the leading trough of the cyclonic edge wave train generated along the west coast propagated to

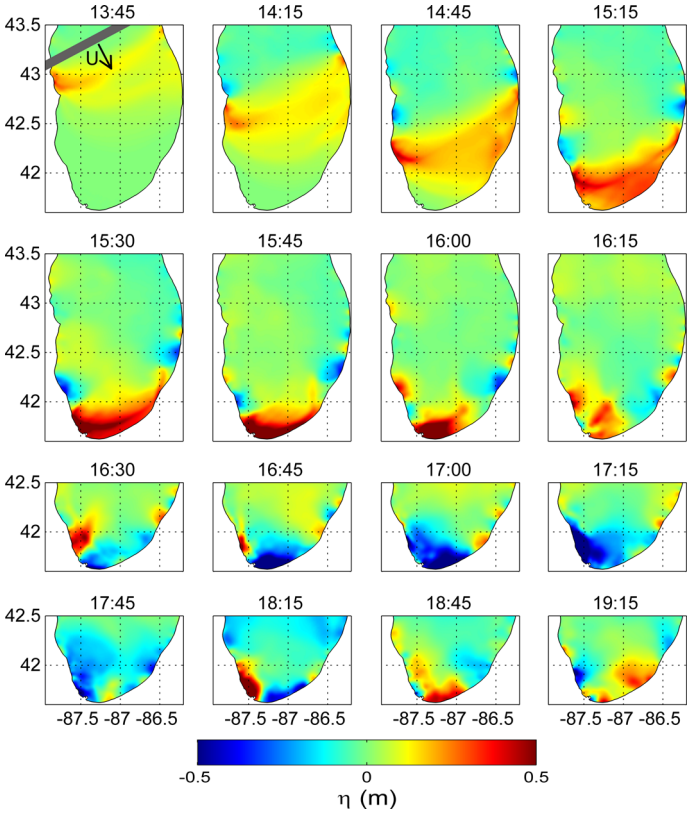

Fig. 9 Lake Michigan water level in response to meteorological forcings on July 6, 1954, from Fig. 3 (times are in CST)

(41.6°N, 87.2°W), while the leading trough of the anticyclonic edge wave train generated along the east coast propagated to (41.9°N, 86.7°W), with the two edge wave trains propagating toward each other. At 16:45, the edge wave trains generated on the east and west coasts met at (41.6°N, 87.3°W) and superposed to a 0.7-m trough. By 17:00, the non-trapped wave trough began to reflect off the southern coast of the lake and was responsible for the 0.6-m trough in the Wilson Avenue Crib water level record (Fig. 8). The cyclonic and anticyclonic edge wave trains further interacted to create a 1.1-m wave trough at (41.6°N, 87.4°W). The subsequent water level fluctuations in the lake were primarily due to the edge waves generated from both the east and west coasts, as the non-trapped wave reflected to the north of Lake Michigan. Of note is an additional superposition of the oppositely propagating edge wave trains which occurred at 18:45 (41.6°N, 87.2°W), where the two distinct edge waves can be seen just after the cyclonic and anticyclonic edge waves met 7 min previously with a resulting crest height of 1.2 m; these edge waves can further be seen propagating away from each other at 19:15, with the cyclonic edge wave at (41.8°N, 86.7°W) and the anticylonic edge wave at (41.6°N, 87.3°W). The edge wave energy persisted in the lake for the duration of the 24-h model run, consistent with the observations of Donn and Ewing (1956).

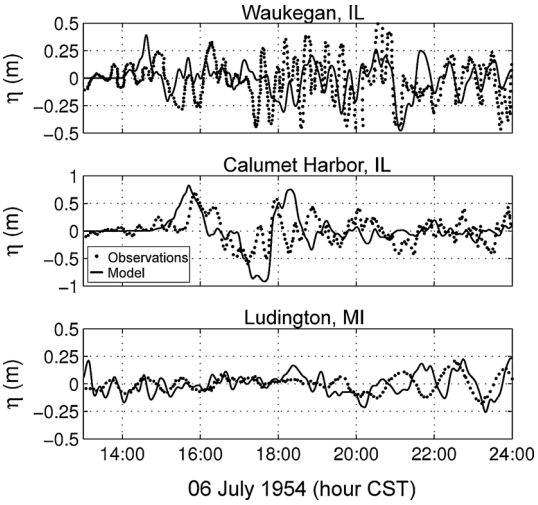

Fig. 10 Time series of modeled water levels (*line*) and observations (*dot*) at shore-based locations throughout Lake Michigan in response to the meteorological forcings on July 6, 1954. For gauge locations, see Fig. 1

To verify the spatial patterns observed in the model snapshots, Fig. 10 compares model results with water level observations reported by Donn and Ewing (1956) at shore-based gauges located at Waukegan, IL; Calumet Harbor, IL; and Ludington, MI (see Fig. 1 for map of locations). Similar to Fig. 6, the shore-based gauges are all located within harbors. As a result, the observed wave signal is likely contaminated by harbor oscillation modes, whereas the model results could not exhibit these effects. At Waukegan, the first wave arrived in the observations at 14:55 with crest height of 0.25 m, consistent with the leading cyclonic edge wave generated on the west coast (Fig. 9, 14:45). The model predicts the edge waves to arrive 15 min earlier at 14:40 with a larger height of 0.4 m. The anticyclonic edge wave train generated on the east coast arrived at Waukegan at 17:14 in the observations with initial wave heights of approximately 0.8 m which diminished to 0.25 m by 22:00. The model depicts this edge wave train arrival 26 min later at 17:40 with smaller heights of 0.5 m persisting for the duration of the model run. The oscillations in the observations occurred at a slightly higher frequency ($T \sim 17$ min) and magnitude ($H \sim 0.8$ m) was compared with the model ($T \sim 22$ min, $H \sim 0.5$ m), though the effects of the harbor may be the source of these discrepancies. At Calumet Harbor (41.7°N, 87.5°W), the leading edge wave arrivals in the observations (18:51) and the model (18:42) were within 10 min, with the observed wave crest height ($H \sim 0.7$ m) slightly smaller than the model ($H \sim 0.8$ m). Subsequent oscillations at Calumet Harbor exhibited similar character in the observations and the model, with the modeled waves slightly larger than in observations. Interestingly, while both Calumet Harbor and Waukegan are near Chicago, the impact of the reflected non-trapped wave which struck Wilson Avenue Crib at 16:45 was not apparent in either record, illustrating the focused and episodic nature of the edge wave/non-trapped wave superposition. At Ludington, early oscillations were small ($H \sim 0.2$ m) in both the observations and the model since the edge waves along the east coast were fairly early in development at this location and had not yet achieved large Greenspan resonant growth. A relatively large wave ($H \sim 0.4$ m) appeared at 18:25 in the model results, associated with the non-trapped wave reflection propagating back northward. The cyclonic edge waves generated on the west coast propagated around the lake and reached Ludington at 21:15 in the observations and 20:40 in the model, with heights

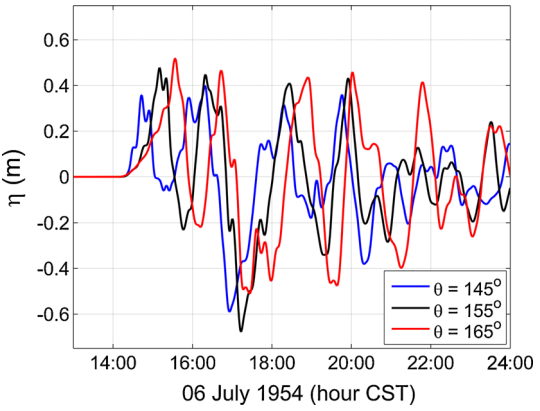

Fig. 11 Time series of water levels at Wilson Avenue Crib in response to perturbation of meteorological disturbance direction for the July 6, 1954 meteotsunami

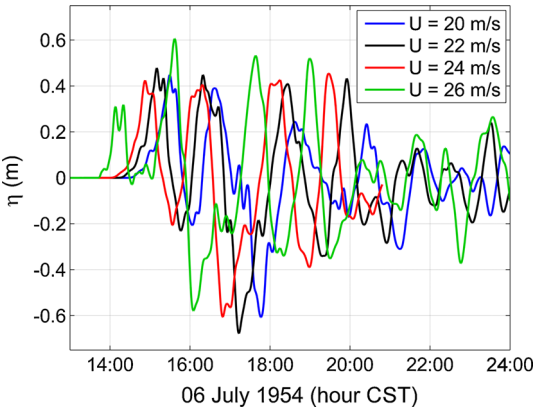

Fig. 12 Time series of water levels at Wilson Avenue Crib in response to perturbation of meteorological disturbance speed for the July 6, 1954 meteotsunami

eventually reaching 0.4 m in the observations and 0.5 m in the model. These oscillations persisted at Ludington for the duration of both the observation and model records. Overall, the model time series reasonably match the observations, with some slight discrepancies in arrival time likely due to the assumed linear atmospheric disturbance front, whereas isochrones suggest that the actual disturbance front may have been slightly curved (Donn and Ewing 1956).

The sensitivity of the July 6th meteotsunami event to atmospheric disturbance velocity is examined by perturbing both propagation direction and speed. While the nomograms of Platzman (1965) provide the maximum wave height in response to a wide range of disturbance velocities, in this paper we aim to examine the detailed wave behavior specific to the July 6th event. First, disturbance direction is perturbed $\pm 10°$ from the original 155°, with the resulting time series at Wilson Avenue Crib plotted in Fig. 11. The more meridional propagation pathway ($\theta = 165°$) results in a later arriving yet a slightly larger initial edge wave at 15:30, owing to the fact that the disturbance propagates closer to direction of edge wave propagation along the coast. Nevertheless, the angle of non-trapped wave reflection changes, which alters the superposition of non-trapped wave and edge wave and results in a 25 % smaller trough height at 17:10. For the more zonal propagation ($\theta = 145°$), the initial edge wave arrives earlier (14:45), but with 75 % of the height of the

base case, the result of the disturbance pathway being less aligned with the alongshore edge wave propagation direction. In comparison with the original base case ($\theta = 155°$), the wave heights in this case are lower (i.e., at 16:55) due to the combination of the reduced edge wave heights and the change in non-trapped wave reflection angle. Overall, the perturbations reveal that edge wave height in this event could have been greater with a more meridional disturbance propagation, but the edge wave/non-trapped wave superposition was maximized at Wilson Avenue Crib for the actual disturbance orientation ($\theta = 145°$).

The atmospheric disturbance speed is perturbed from the original 22 m/s in 2 m/s increments, yielding 20, 24, and 26 m/s disturbances, with a comparison of the resulting water levels at Wilson Avenue Crib plotted in Fig. 12. The slower disturbance ($U = 20$ m/s) results in later arriving (15:29) and slightly smaller water level fluctuations, with mechanisms similar to the base case. The slightly faster disturbance ($U = 24$ m/s) leads to an earlier arriving wave train (14:53) with a 10 % smaller height, likely owing to a deviation from the ideal Greenspan resonant speed. An appreciable change in behavior is observed for $U = 26$ m/s, in which a 66 % smaller initial edge wave occurs at 14:18, as this disturbance speed further departs from the Greenspan resonant edge wave speed. Nevertheless, the faster disturbance speed approaches the Proudman resonant speed for the open water of Lake Michigan ($c = 29$ m/s), so a much larger wave is generated, reflecting back to the gauge at 15:38 with a 0.6 m crest height. At this disturbance speed, the hypothetical meteotsunami event would be attributed primarily to the non-trapped wave instead of edge waves, drawing more similarities to the June 26th wave than the July 6th event under consideration. Overall, the sensitivity study of the July 6th event conducted here reveals that changes in disturbance speed and direction can dramatically affect the character of meteotsunami wave produced, including changing the dominant wave type.

4 Discussion

4.1 Role of edge waves and non-trapped waves

The modeling results, in particular the snapshots in Figs. 5 and 9, uncover that both events generated non-trapped waves and edge waves simultaneously in Lake Michigan. Previously, Donn (1959) described an atmospheric disturbance on the Great Lakes which generated edge waves on Lake Huron and non-trapped waves in Lake Erie, owing to the disturbance orientation relative to the shorelines of each lake. Nevertheless, simultaneous generation of edge waves and non-trapped waves on the same lake has yet to be documented as far as the authors are aware. While edge waves did not play a major role in the destructive wave that struck Chicago in the June 26th event, significant oscillations ($H > 0.5$ m) due to edge waves occurred hours after the initial wave. These persistent large waves were noted in witness accounts to hinder rescue and recovery efforts for hours after the deadly wave. The late arrival of these waves would have had no apparent connection to the squall line storm that had passed hours earlier and may have posed a threat to public safety had beaches not been cleared due to the fatal non-trapped wave. In the July 6th event, the largest wave observed was the result of edge wave and non-trapped wave superposition. The superimposed edge wave and non-trapped wave resulted in a peak water level 60 % larger than the other waves in the edge wave train. Nevertheless, the presence of the non-trapped wave was not considered in the original analysis of Donn and Ewing (1956) because large Proudman resonance was ruled out as a source, owing to the slower

disturbance speed. The hydrodynamic model results presented in this paper indicate that edge waves and non-trapped waves can be generated simultaneously by the same disturbance despite the fact that these waves may not achieve an optimal resonant condition. Indeed, interaction between long and edge waves can create a destructive event, as occurred on July 6, 1954. Therefore, the study of future events in Lake Michigan and other enclosed basins is highly recommended to take both long and edge waves into consideration.

4.2 Effects of an enclosed basin

The simultaneous appearance of both edge waves and non-trapped waves in the two events can be attributed in part to the enclosed basin of Lake Michigan. For non-trapped waves, the enclosed basin allows for reflection and subsequent retention of wave energy in the southern basin of the lake. In addition, the concave shape of the east coast of Lake Michigan acts to focus on the reflected non-trapped waves propagating westward, as illustrated in Fig. 5. This spatial focusing can result in a reflected wave on the west coast of the lake which exceeds the wave incident at the east coast, as occurred on June 26, 1954. This type of directional spatial focusing is one of the mechanisms identified to cause freak waves (Nepf et al. 1998; Wu and Nepf 2002; Kharif and Pelinosvsky 2003). Edge waves can persist for long durations as they travel around an enclosed coast, evident in the late wave arrivals on the west coast by anticyclonic edge waves generated on the east coast for the June 26 event. If edge waves are generated on both coasts, the two edge wave trains may meet and interact, as seen in Fig. 9 for July 6, 1954, at 16:45 (41.6°N, 87.3°W) and 18:45 (41.6°N, 87.2°W). The resulting waves in this case were rather large, with the superposition leading to waves in excess of 1 m crest height in some cases. The enclosed nature of the Lake Michigan basin makes these meteotsunamis unique and potentially more dangerous compared to meteotsunamis along an ocean or sea coast where wave reflection and propagation lead to energy leaving the area of concern.

4.3 Wind stress versus atmospheric pressure

While the potential of wind stress to significantly contribute to meteotsunami height has been recognized (Vilibić et al. 2005; Orlić et al. 2010), in events studied to date wind stress has been viewed as a secondary forcing compared to atmospheric pressure (Šepić et al. 2008; Orlić et al. 2010; Renault et al. 2011). Coincidentally, the previous studies of these Lake Michigan meteotsunamis did not consider wind stress to be significant. The description of the July 6th event by Donn and Ewing (1956) merely mentioned that wind speeds exceeded 30 m/s, whereas the modeling exercise by Platzman (1958) on the June 26 meteotsunami event only considered atmospheric pressure and neglected to account for wind stress. The generic modeling results of Platzman (1965) indicated the potential for wind stress to dominate meteotsunami wave behavior, though not for a specific event. The model results in our study indicate that wind stress was responsible for 40 and 68 % of the wave heights in the June 26 and July 6 events, respectively. Clearly, wind disturbance can play a significant role in generating meteotsunamis in Lake Michigan. It is also important to note that the observed wind speeds of 25 and 32 m/s for June 26 and July 6, respectively, are much greater than that of any other meteotsunami discussed in the literature. This may be an indication that squall line storms, which are characterized by strong winds (Rotunno et al. 1988; Wakimoto et al. 2006), may be a meteotsunami source unique to the Great Lakes. Furthermore, the occurrence of derechos, which are strong squall lines, has risen

recently in the USA from approximately 10 events per year in 1986 to about 30 events per year by 2003 (Ashley et al. 2005), with the lower Great Lakes region emerging as a dominant corridor of derecho activity at the end of the twentieth century (Bently and Sparks 2003). An increase in the number and severity of high-speed squall line events suggests the potential for more frequent and intense Great Lakes meteotsunamis in the near future.

5 Summary

In this paper, two distinct meteotsunami events that occurred on Lake Michigan in 1954 were revisited using a hydrodynamic modeling approach. Data analysis immediately following the events concluded that first event (June 26) was caused by Proudman resonance between a non-trapped wave and a squall line (Ewing et al. 1954), whereas the second event (July 6th) was attributed to Greenspan resonance between a propagating pressure jump and an edge wave train (Donn and Ewing 1956). Nevertheless, the high-resolution hydrodynamic modeling results in this paper reveal details on these two events that the early modeling did not resolve, including the role of pressure and wind stress on meteotsunami formation, the character of the wave growth, significant higher-frequency content present in the waves, and the long duration of the water level oscillations.

On June 26, 1954, a squall line with a rapid pressure jump and strong winds propagated southeast across the lake. The squall line propagation speed, approximately equal to the wave speed in southern Lake Michigan, led to Proudman resonance that amplified a non-trapped wave. When this non-trapped wave struck the east and south coasts of the lake, the wave reflected back west and, owing to the curvature of the shore, focused on the wave front at the Chicago lakeshore. While the main wave front had a period of 90 min, observations revealed what appeared to be high-frequency component ($T = 15$ min) to this wave, termed a "second surge" by Ewing et al. (1954); the model results indicate that this apparent high-frequency content was actually the reflection of the destructive wave off of the west coast and not a complex high-frequency wave front as originally conjectured. Furthermore, model results reveal waves that arrived hours after the first wave struck Chicago were associated with a harmonic edge wave generated on the east coast of the lake by the squall line. The edge waves then propagated anticyclonically around the lake to impact the Chicago lakefront hours after the non-trapped wave energy had dissipated. Though the non-trapped wave was the cause of the fatal meteotsunami that struck Chicago, the significant edge wave energy persisted in the lake for a long duration, proving a hindrance to rescue missions and a potential danger owing to the arrival long after the squall line and non-trapped wave had passed.

Ten days later on July 6, another series of large waves struck the Chicago coast. Initially attributed to edge wave resonance by Donn and Ewing (1956), model simulations reveal that the largest of these waves was the product of a resonant edge wave superposed with the reflected non-trapped wave. This outcome stresses the role that the enclosed basin of Lake Michigan played in creating a complex wave environment, as a significant portion of the wave energy was retained through reflection compared to the open sea condition. In addition, high-frequency oscillations observed with the large waves were attributed to first harmonic edge wave modes. Another major finding was that the main source of energy for this event was wind stress, which is contrary both to the initial hypothesis of Donn and Ewing (1956) and the conventional conclusion in the meteotsunami literature that pressure

gradient is the main driver of these large waves. Indeed, the importance of wind stress in both of the events examined in this study may indicate that the squall line storms that generate Great Lakes meteotsunamis may be fundamentally different from meteotsunami-causing storms elsewhere in the world.

Acknowledgments This work was supported by the National Science Foundation's Graduate Research Fellowship Program, the Cooperative Institute for Limnology and Ecosystems Research Long-term Great Lakes Fellowship, and UW-Madison/UW-Milwaukee Intercampus Research Incentive Grants Program. The authors would like to thank Dr. David Schwab at the University of Michigan-Ann Arbor and Dr. Eric Anderson at NOAA-Great Lakes Environmental Research Laboratory for the advice and discussion on meteotsunamis in the Great Lakes. The authors would also like to thank the two anonymous reviewers whose comments greatly improved the manuscript. At last, the authors greatly thank Dr. Ivica Vilibic, Dr. Alexander B. Rabinovich, and Dr. Sebastian Monserrat for their endeavors to make the special issue on meteorological tsunamis come true. Furthermore, their leadership and contribution to this important topic is highly acknowledged.

References

Ashley WS, Mote TL, Bentley ML (2005) On the episodic nature of derecho-producing convective systems in the United States. Int J Climatol 25:1915–1932

Bently ML, Sparks JA (2003) A 15 year climatology of derecho-producing mesoscale convective systems over the central and eastern United States. Clim Res 24:129–139

Cho KH, Wang HV, Shen J, Valle-Levinson A, Teng YC (2012) A modeling study on the response of the Chesapeake Bay to Hurricane Events of Floyd and Isabel. Ocean Model 49–50:22–46

Donelan MA, Haus BK, Reul N, Plant WJ, Stiassnie M, Graber HC, Brown OB, Saltzman ES (2004) On the limiting aero-dynamic roughness of the ocean in very strong winds. Geophys Res Lett 31:L18306. doi:10.1029/2004GL019460

Donn WL (1959) The Great Lakes storm surge of May 5, 1952. J Geophys Res 64(2):191–198

Donn WL, Ewing M (1956) Stokes' edge waves in Lake Michigan. Science 124(3234):1238–1242

Ewing M, Press F, Donn WJ (1954) An explanation of the Lake Michigan wave of 26 June 1954. Science 120(3122):684–686

Fortunato AB, Rodrigues M, Dias JM, Lopes C, Oliveira A (2013) Generating inundation maps for a coastal lagoon: a case study in the Ria de Aveiro (Portugal). Ocean Eng 64:60–71

Greenspan HP (1956) The generation of edge waves by moving pressure disturbances. J Fluid Mech 1:574–592

Harris DL (1957) The effect of a moving pressure disturbance on the water level in a lake. Meteorol Monogr 2(10):46–57

Hibiya T, Kajiura K (1982) Origin of "abiki" phenomenon (kind of seiches) in Ngasaki Bay. J Oceanogr Soc Jpn 38:172–182

Hughes LA (1965) The prediction of surges in the southern basin of Lake Michigan: part III. The operational basis for prediction. Mon Weather Rev 93(5):292–296

Kelley JGW, Hobgood JS, Bedford KW, Schwab DJ (1998) Generation of three-dimensional lake model forecasts for Lake Erie. Weather Forecast 13(3):659–687

Kharif C, Pelinosvsky E (2003) Physical mechanisms of the rouge wave phenomenon. Eur J Mech B Fluids 22(6):603–634

Kurkin A, Pelinovsky E (2003) Shallow-water edge waves above an inclined bottom slowly varied in alongshore direction. Eur J Mech B Fluids 22(4):305–316

Monserrat S, Vilibic I, Rabinovich AB (2006) Meteotsunamis: atmospherically induced destructive ocean waves in the tsunami frequency band. Nat Hazards Earth Syst Sci 6(6):1035–1051

Munk W, Snodgrass F, Carrier G (1956) Edge waves on the continental shelf. Science 123(3187):127–132

Nepf HM, Wu CH, Chan ES (1998) A comparison of two- and three-dimensional wave breaking. J Phys Oceanogr 28(7):1496–1510

O'Connor WP, Schwab DJ, Lang GA (1999) Forecast verification for eta model winds using Lake Erie storm surge water levels. Weather Forecast 14(1):119–133

Orlić M, Belusic D, Janekovic I, Pasaric M (2010) Fresh evidence relating the great Adriatic surge of 21 June 1978 to mesoscale atmospheric forcing. J Geophys Res 115. doi:10.1029/2009JC005777

Platzman GW (1958) A numerical computation of the surge of 26 June 1954 on Lake Michigan. Geophysica 6(1):407–438
Platzman GW (1965) The prediction of surges in the southern basin of Lake Michigan: part I. The dynamical basis for prediction. Mon Weather Rev 93(5):275–281
Powell MD, Vickery PJ, Reinhold TA (2003) Reduced drag coefficient for high wind speeds in tropical cyclones. Nature 422:279–283
Proudman J (1929) The effects on the sea of changes in atmospheric pressure. Geophys Suppl Mon Not R Astron Soc 2(4):197–209
Rabinovich AB (2009) Seiches and harbor oscillations. In: Kim YC (ed) Handbook of coastal and ocean engineering. World Scientific, Singapore, pp 193–236
Renault L, Vizoso G, Jansá A, Wilkin J, Tintoré J (2011) Toward the predictability of meteotsunamis in the Balearic Sea using regional nested atmosphere and ocean models. Geophys Res Lett 38. doi:10.1029/2011GL047361
Rotunno R, Klemp JB, Weisman ML (1988) A theory for strong, long-lived squall lines. J Atmos Sci 45(3):463–485
Šepić J, Orlić M, Vilibić I (2008) The Bakar Bay seiches and their relationship with atmospheric processes. Acta Adriat 49(2):107–123
Sheppard PA (1958) Transfer across the earth's surface and through the air above. QJR Meteorol Soc 84:205–224
Smith SD (1980) Wind stress and heat flux over the ocean in gale force winds. J Phys Oceanogr 10:709–726
Song Y, Haidvogel D (1994) A semi-implicit ocean circulation model using a generalized topography-following coordinate system. J Comput Phys 115(1):228–244
Ursell F (1952) Edge waves on a sloping beach. Proc R Soc Ser A 214(1116):79–98
Vilibić I (2008) Numerical simulations of the Proudman resonance. Cont Shelf Res 28:574–581. doi:10.1016/j.csr.2007.11.005
Vilibić I, Domijan N, Cupic S (2005) Wind versus air pressure seiche triggering in the Middle Adriatic Coastal waters. J Mar Sci 57(1–2):189–200
Vilibić I, Monserrat S, Rabinovich A, Mihanovic H (2008) Numerical modeling of the destructive meteotsunami of 15 June, 2006 on the coast of the Baleric Islands. Pure Appl Geophys 165:2169–2195. doi:10.1007/s00024-008-0426-5
Wakimoto RM, Murphey HV, Nester A, Jorgensen DP, Atkins NT (2006) High winds generated by bow echoes. Part I: overview of the Omaha bow echo 5 July 2003 storm during BAMEX. Mon Weather Rev 134(10):2793–2812. doi:10.1175/MWR3215.1
Witter RC, Jaffe B, Zhang Y, Priest GR (2011) Reconstructing hydrodynamic flow parameters of the 1700 tsunami at Cannon Beach, Oregon, USA. Nat Hazards. doi:10.1007/s11069-011-9912-7
Wu CH, Nepf HM (2002) Breaking wave criteria and energy losses for three-dimensional breaking waves. J Geophys Res Oceans 107(C10):41-1–41-18. doi:10.1029/2001JC001077
Zhang Y, Baptista AM (2008a) SELFE: a semi-implicit Eulerian–Lagrangian finite-element model for cross-scale ocean circulation. Ocean Model 21(3–4):71–96
Zhang Y, Baptista AM (2008b) An efficient and robust tsunami model on unstructured grids. Part I: inundation Benchmarks. Pure Appl Geophys 165(11–12):2229–2248
Zhang Y, Witter RW, Priest GP (2011) Tsunami–tide interaction in 1964 Prince William Sound tsunami. Ocean Model 40(3–4):246–259